Dalton Transactions

PAPER

View Article Online
View Journal | View Issue

Cite this: *Dalton Trans.*, 2014, **43**, 17108

Unraveling the origins of catalyst degradation in non-heme iron-based alkane oxidation†

Michaela Grau, Andrew Kyriacou, Fernando Cabedo Martinez, Irene M. de Wispelaere, Andrew J. P. White and George J. P. Britovsek*

Received 8th July 2014,
Accepted 30th September 2014

DOI: 10.1039/c4dt02067g

www.rsc.org/dalton

A series of potentially tetradentate and pentadentate ligands modelled on BPMEN has been prepared and their iron(II) bis(triflate) complexes have been isolated and characterised by spectroscopic and crystallographic techniques (BPMEN = *N*,*N*′-bis(pyridylmethyl)ethylenediamine). Changes to the BPMEN ligand have invariably led to complexes with different coordination modes or geometries and with inferior catalytic efficiencies for the oxidation of cyclohexane with H_2O_2. The reaction of an iron(II) complex containing a pentadentate BPMEN-type ligand with O_2 has resulted in ligand degradation *via* oxidative N-dealkylation and the isolation of a bis(hydroxo)-bridged dinuclear iron(III) complex with a picolinate-type ligand.

Introduction

Catalyst deactivation is a common but often ignored problem in catalyst development, in particular in oxidation catalysis. Oxidative ligand degradation of a homogeneous molecular oxidation catalyst during its lifetime can be a limiting factor for high turnover and the activity of the catalyst is often directly related to its stability under the oxidising reaction conditions.[1] In living systems, ligand degradation of oxidation catalysts also occurs in enzymatic systems where both heme and non-heme oxidases have a limited lifetime, but are regenerated *in vivo* by complex mechanisms.[2,3]

A thorough understanding of the various oxidative ligand degradation processes will be essential for the design and development of more robust oxidation catalysts. In heme-based oxidation catalysts, one mode of deactivation has been shown to involve oxidation of the porphyrin ligand.[4–8] While the exact deactivation pathway in the large variety of non-heme metal catalysts is not known at this stage, oxidative degradation of the ligand is probably one of the main causes for catalyst deactivation. Another possible deactivation pathway that has been invoked in a number of non-heme catalyst systems is the formation of inactive dinuclear μ-oxo iron(III) complexes.[9,10]

Various oxidative ligand degradation pathways have been observed in non-heme iron systems, for example peripheral alkyl and aryl C–H bond oxidations,[11–13] and more importantly for amine-based ligands, *oxidative N-dealkylation*. The cleavage of C–N bonds in metal complexes with polydentate amine ligands *via* oxidative N-dealkylation is a general problem that has been observed on many occasions.[14–16] After initial oxidation of Fe(II) to Fe(III), the C–H bonds adjacent to an amine moiety (CHR–NR′$_2$) (**A** in Scheme 1) are prone to oxidation resulting in the formation of hemi-aminal (C(OH)R–NR′$_2$) complexes (**B**).[17] Particularly vulnerable to oxidative degradation

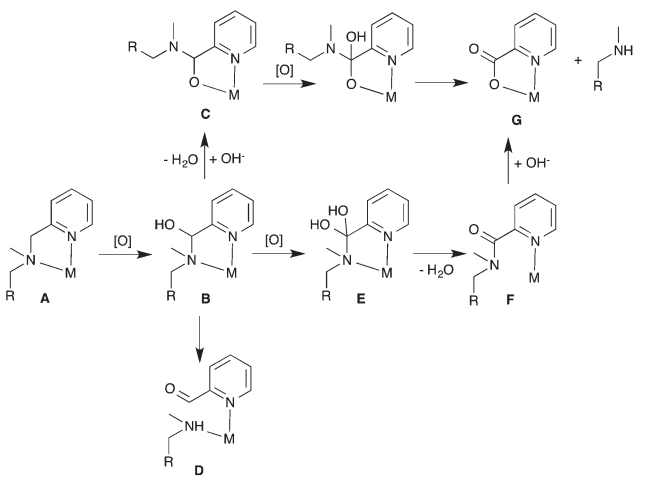

Scheme 1 Potential degradation pathways *via* oxidative N-dealkylation in pyridylmethyl amine complexes ([O] = oxidation).

Department of Chemistry, Imperial College London, Exhibition Road, London, SW7 2AZ, UK. E-mail: g.britovsek@imperial.ac.uk; Fax: +44-(0)20-75945804; Tel: +44-(0)20-75945863

†Electronic supplementary information (ESI) available: X-ray crystallographic files in CIF format and experimental details regarding the synthesis and characterisation of the ligands and metal complexes, including spectroscopic details. CCDC 995554–995556. For ESI and crystallographic data in CIF or other electronic format see DOI: 10.1039/c4dt02067g

are methylene or methine protons adjacent to an amine that are also in alpha position to a carbonyl group, for example in amino acids,[18–21] or next to an aromatic unit such as phenyl (benzylic),[22–25] phenolate,[26] or pyridine moieties, as shown in Scheme 1.[27–34] Occasionally, the hemi-aminal products are stable enough and can be isolated as O-bound hemi-aminal complexes of type **C**.[35–39] Alternatively, hemi-aminals are prone to dissociation into an aldehyde (or ketone) and a secondary amine (**D**).[40] In many cases where ligand degradation has occurred *via* oxidative N-dealkylation, degradation products such as aldehydes,[23–25,41–44] or ketones[30,45] have been isolated. A third possibility is further oxidation of the hemi-aminal intermediate (**B**) to an amide complex (**F**). Hydrolysis of this amide intermediate would result in the formation of picolinic acid from pyridylmethylamine moieties, which appears to be a common occurrence, sometimes resulting in the formation of stable metal picolinate complexes (**G**).[42,44,46,47]

The prevention of oxidative ligand degradation is an on-going challenge in the design of more efficient oxidation catalysts. In an attempt to prepare more robust biomimetic catalysts for the oxidation of alkanes, we have previously reported various derivatives of the benchmark catalyst [Fe(BPMEN)(OTf)$_2$],[48–50] developed by Que and co-workers (BPMEN = *N*,*N*′-bis(pyridylmethyl)ethylenediamine).[51] The selectivity and stability of [Fe(BPMEN)(CH$_3$CN)$_2$](SbF$_6$)$_2$ is improved by adding electron donating *para*-methoxy groups to the pyridine moieties of the BPMEN ligand.[50,52] Electron donating ligands are preferred because they can support high-valent iron oxo intermediates, which are generally assumed to be the active oxidant in these systems.

Our continuing efforts to understand and improve the stability of non-heme iron-based catalyst have led us to explore three aspects of the BPMEN ligand. Firstly, the effect of N–Me *versus* N–H substitution in alkane oxidation has been evaluated (ligand **1**, Fig. 1). Complexes containing secondary amines are generally prone to oxidative dehydrogenation under oxidising conditions and therefore would be expected to give a poorer performance.[53–55] Secondly, methylene (CH$_2$) moieties adjacent to amine donors have been identified as vulnerable to oxidation.[17] To avoid such methylene linkages, we have prepared tetradentate ligands with a C(Me)H or a C=O linkage between the pyridine and the amine donor (ligands **2–4**). Replacing vulnerable C–H bonds with C–Me bonds has previously been used to improve the catalyst stability in other non-heme catalysts,[56] and a recent report on a related iron(II) catalyst with C(Ph)H linkages has shown promising results in asymmetric epoxidations.[57] In a third series, we have explored the application of linear pentadentate ligands in oxidation catalysis (**5–8**). An additional donor could result in greater catalyst stability and within this series we have examined the effect of N–H (**5**) *versus* N–Me substitution (**6**), the removal of CH$_2$ linkages (**7**) and an alternative donor set (**8**) on the catalytic behaviour in cyclohexane oxidation.

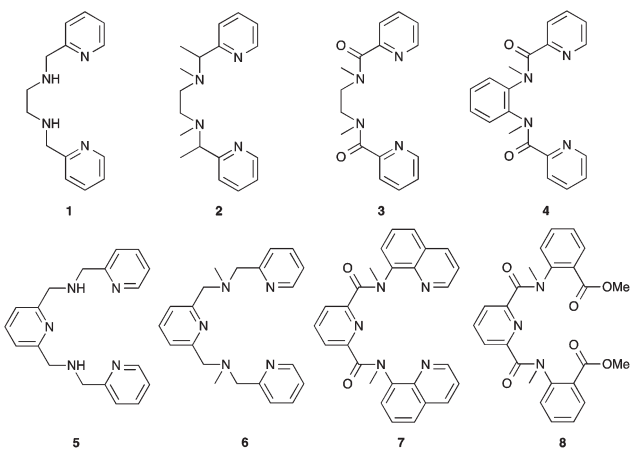

Fig. 1 Overview of tetradentate and pentadentate pyridylmethylamine ligands (**1–8**).

Results and discussion

Synthesis and characterisation of ligands and metal complexes

The *N*-methylated pyridylamine ligands **2** and **6** were prepared from the non-methylated precursors.[58–62] The *N*-methyl carboxamide ligands **3**, **4**, **7** and **8** were prepared by methylation of the carboxamides, which were obtained by reacting pyridine dicarboxylic acid or acid chloride with the corresponding amine (see Experimental section). *N*-methyl carboxamides show restricted rotation around the CO–NMe bond, which can lead to 3 rotamers and complicated NMR spectra.[63] The ratio between the three different rotamers was determined as 4 : 3 : 3 in the case of ligand **3**, as reported previously.[64] For the new ligands **4**, **7** and **8**, the ratio was determined as 10 : 6 : 1 for ligand **4** (Fig. S1†) and as 3 : 2 : 1 for ligand **8**. Only one isomer was observed for ligand **7** (Fig. S2†).

The iron(II) bis(triflate) complexes were prepared by combining the ligands and [Fe(OTf)$_2$(MeCN)$_2$] in THF as the solvent. The complex [Fe(BPMEN)(OTf)$_2$] has a *cis*-α coordination mode in the solid state and according to VT-^{19}F NMR studies, there is no fluxional coordination behaviour in CD$_2$Cl$_2$ solution between 233–298 K.[50] In acetonitrile solution, the cationic complex [Fe(BPMEN)(CH$_3$CN)$_2$]$^{2+}$ is formed,[51,65] which shows a temperature dependant $^5T_2 \rightarrow {}^1A_1$ spin crossover (SC) behaviour with μ_{eff} = 1.1μ_B at 233 K and μ_{eff} = 5.1μ_B at 343 K (T_c = 264 K) in acetonitrile (see (■) Fig. 2).[50,66]

In contrast, the non-methylated complex [Fe(**1**)(OTf)$_2$] shows a different behaviour. This complex also forms a dicationic complex [Fe(**1**)(CH$_3$CN)$_2$]$^{2+}$ in acetonitrile,[67] which was recently crystallographically characterised at 100 K as a low spin complex with *cis*-α coordination.[68] However, we noticed that the signals for this complex in the ^{1}H NMR spectrum in CD$_3$CN are unusually broad at room temperature and more species are observed at higher temperatures (see Fig. S3†). Complex [Fe(**1**)(CH$_3$CN)$_2$]$^{2+}$ undergoes SC approximately at room temperature, due to the strong field acetonitrile ligands (see Fig. 2 (▲) and VT-^{1}H NMR spectra in Fig. S4†). For comparison, the complex [Fe(**1**)(SCN)$_2$] with relatively weak field

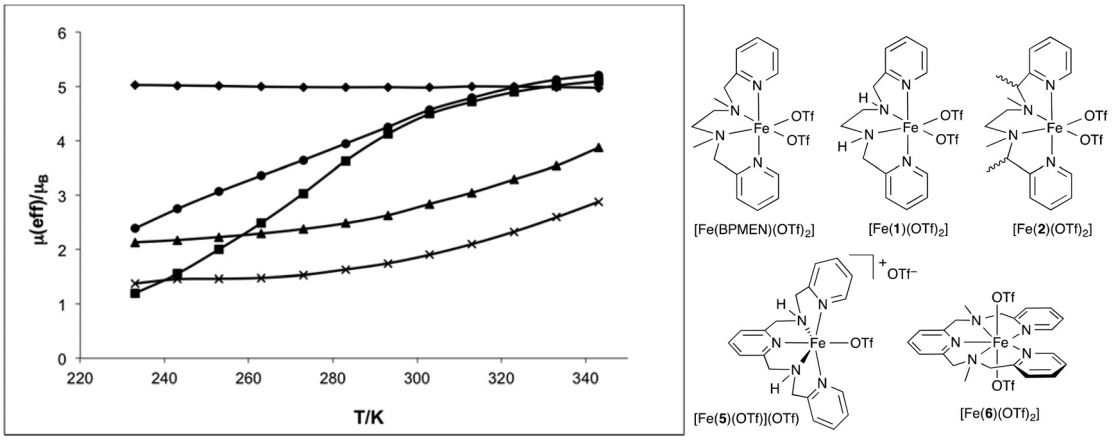

Fig. 2 Magnetic moment (μ_{eff}) *versus* temperature in CD_3CN for complexes [Fe(BPMEN)$(OTf)_2$] (■), [Fe(**1**)$(OTf)_2$] (▲), [Fe(**2**)$(OTf)_2$] (●), [Fe(**5**)(OTf)](OTf) (×), [Fe(**6**)$(OTf)_2$] (◆).

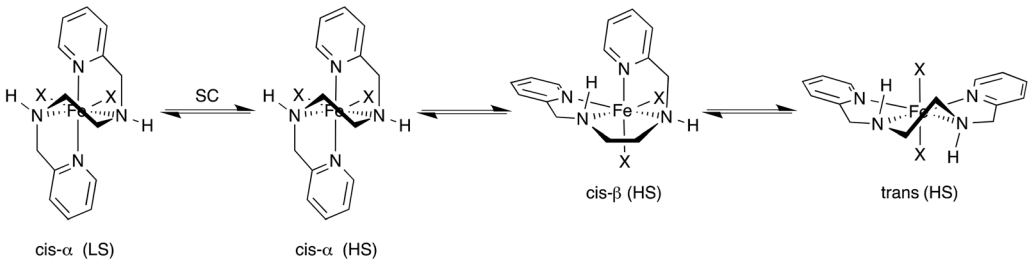

(1)

thiocyanate ligands undergoes $^5T_2 \rightarrow {}^1A_1$ relaxation at a very low transition temperature of 70 K,[69] and later studies have revealed a very slow spin transition process in the solid state.[70] Compared to [Fe(BPMEN)$(CH_3CN)_2]^{2+}$, the change in magnetic susceptibility of [Fe(**1**)$(CH_3CN)_2]^{2+}$ is much more gradual with $\mu_{eff} = 2.1\mu_B$ at 233 K and $\mu_{eff} = 3.9\mu_B$ at 343 K (Fig. 2). This suggests that [Fe(**1**)$(CH_3CN)_2]^{2+}$ undergoes geometrical changes with temperature, most likely to form other HS complexes with different geometries. Geometrical rearrangements of iron(II) complexes with tetradentate ligands similar to ligand **1** are quite common and we have seen isomerisation between *cis*-α and other geometries *cis*-β and *trans*, for example when the chelate rings size or donor strength has been changed.[49,50] Here, the weaker basicity of the N–H *versus* N–Me donor and the resulting weaker Fe–N bond strength, results probably in a similar rearrangement process. For example the analogous complex with O instead of NH donors forms the *trans* complex exclusively.[50] Noteworthy, *cis*-β and *trans* geometries are known for ligand **1** with different metals such as Co(III) and Cr(III).[71–74] The activation barriers ($\Delta H^{\ddagger}$) for spin transitions between HS and LS iron(II) complexes can vary in solution between 2 and 34 kJ mol^{-1} and may become competitive with geometric rearrangements.[75,76] Coupling between the spin relaxation process and the geometrical rearrangement of the ligand, as seen in a related system,[77] cannot be excluded.

VT-^{19}F NMR analysis of complex [Fe(**1**)$(OTf)_2$] in CD_2Cl_2 shows a broad signal at −40 ppm at room temperature, which coalesces at 258 K and reveals multiple species in equilibrium, most likely *cis*-β and *trans* isomers in addition to the main *cis*-α complex (see Fig. S5†). We conclude that the non-methylated complex [Fe(**1**)$(OTf)_2$] must be conformationally less rigid compared to [Fe(BPMEN)$(OTf)_2$], probably due to the weaker basicity of NH *versus* NMe donors. The ligand flexibility results in a combination of spin crossover and geometric isomerisation upon changing the temperature, which explains the anomalous magnetic behaviour seen in Fig. 2.

Ligand **2**, with two chiral centres, forms a pair of enantiomers (*R*,*R* and *S*,*S*) and a meso form (*R*,*S* or *S*,*R*). Upon coordination to the iron(II) centre, two additional N-chirogenic centres are created at the amino nitrogen atoms. This could result in 16 isomers, but the *cis*-α coordination mode only supports the [(N)*S**,(N)*S**] configuration at the central amine donors. This reduces the number of possible isomers to 8 (4 pairs of enantiomers). The four possible isomers with [(N)*S*,(N)*S*] configuration at the central amines are shown in Fig. 3. The two *meso* isomers **C** are identical, which reduces the number of complexes to three diastereomeric complexes **A**, **B** and **C** in a 1 : 1 : 2 ratio.

The presence of diastereomers complicates the ^{1}H NMR spectrum of [Fe(**2**)$(OTf)_2$] in CD_3CN. At 228 K, the spectrum appears to consist of a mixture of two complexes (or groups of

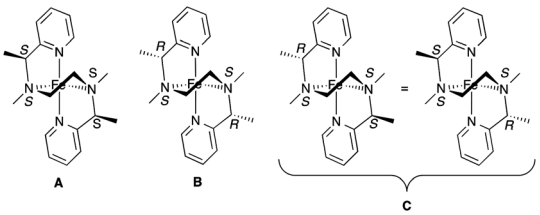

Fig. 3 Four of eight possible isomers for complex [Fe(**2**)$(OTf)_2$] with *cis*-α geometry (the OTf^- ligands have been omitted for clarity).

complexes), which we presume are **A** and **B** on the one hand, and **C** on the other (see Fig. S6†). One complex is diamagnetic at this temperature, with a chemical shift range between 0 and 10 ppm and the other is partially high spin (HS) with a shift range from −5 to 40 ppm. The latter complex is fully HS at 278 K and follows Curie behaviour upon further temperature increase. The spin crossover temperature for this complex is at $T_c \approx 200$ K. The diamagnetic complex shows 9 signals at 228 K and as the temperature is raised, undergoes spin crossover at $T_c \approx 235$ K, whereby the chemical shift range increases and the signals become gradually broader. At 288 K, the signals for this complex are extremely broad, due to exchange between coordinated and non-coordinated CD_3CN ligands. At the highest temperature of 338 K, the exchange is sufficiently fast for the signals to sharpen again. From 298 K onwards, all complexes are paramagnetic and follow Curie behaviour with further temperature increase. VT ^{19}F NMR spectroscopy (Fig. S8†) and magnetic susceptibility measurements (see (●) in Fig. 2) also indicate a different behaviour compared to [Fe(BPMEN)$(OTf)_2$], indicative of multiple complexes, each with a different spin crossover behaviour and T_c values.

The complexes [Fe(**3**)$(OTf)_2$] and [Fe(**4**)$(OTf)_2$] are high spin over the temperature range from 243–343 K, according to VT-^{1}H-NMR studies. The NMR spectra are rather complicated (see for example Fig. S10†) and indicate the presence of more than one species in solution, possibly different isomers due to the different ligand rotamers. IR spectroscopy shows a change in ν(C═O) from 1636 and 1648 cm^{-1} for **3** and **4**, respectively, to 1608 and 1610 cm^{-1} for the corresponding iron(II) complexes, indicating coordination of the carbonyl oxygen, which is not uncommon in picoline amide ligands.[27,78] In the case of complex [Fe(**4**)$(OTf)_2$], X-ray quality crystals were obtained from a THF solution and analysis revealed the formation of a dinuclear complex [Fe(**4**)$(OTf)_2]_2$ with carbonyl oxygen coordination and the ligand binding in a bridging bis(bidentate) mode (see Fig. 4 and 5). The dinuclear complex has adopted a C_2 symmetric geometry about an axis that passes through the middle of the $Fe_2O_4N_4C_8$ macrocycle. Each iron centre has a distorted octahedral geometry with *cis* angles in the range 75.19(5)–102.84(5)°, and is bound to two bidentate *N*,*O* donor ligands as well as two triflate groups. The only π–π stacking interaction of note is an intramolecular contact between the N(18) pyridyl ring and its C_2 related counterpart

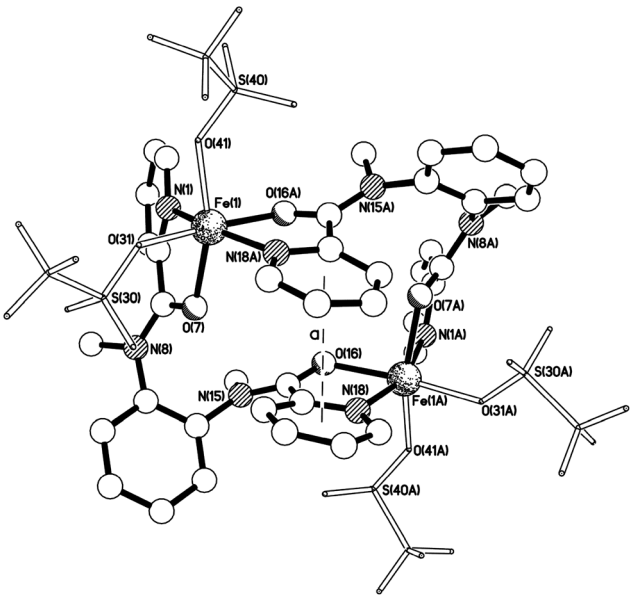

Fig. 4 The crystal structure of the C_2-symmetric complex [Fe(**4**)$(OTf)_2]_2$. Selected bond lengths (Å) and angles (°); Fe(1)–N(1) 2.1674(15), Fe(1)–O(7) 2.1769(13), Fe(1)–O(31) 2.0948(13), Fe(1)–O(41) 2.1100(14), Fe(1)–O(16A) 2.0964(11), Fe(1)–N(18A) 2.1632(14), N(1)–Fe(1)–O(7) 75.19(5), N(1)–Fe(1)–O(31) 102.84(5), N(1)–Fe(1)–O(41) 88.85(6), N(1)–Fe(1)–O(16A) 86.60(5), N(1)–Fe(1)–N(18A) 161.27(5), O(7)–Fe(1)–O(31) 88.21(5), O(7)–Fe(1)–O(41) 161.14(5), O(7)–Fe(1)–O(16A) 94.02(5), O(7)–Fe(1)–N(18A) 99.13(5), O(31)–Fe(1)–O(41) 85.60(6), O(31)–Fe(1)–O(16A) 170.56(5), O(31)–Fe(1)–N(18A) 94.70(5), O(41)–Fe(1)–O(16A) 94.98(5), O(41)–Fe(1)–N(18A) 99.12(6), O(16A)–Fe(1)–N(18A) 75.90(5).

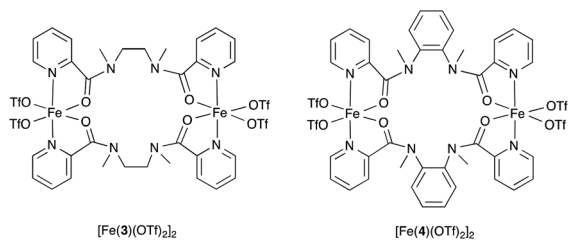

Fig. 5 Molecular structures of iron(II) bis(triflate) complexes of ligands **3** and **4**.

with centroid···centroid and mean interplanar separations of *ca.* 3.67 and 3.61 Å, the two rings inclined by *ca.* 12° (interaction **a** in Fig. 4).

We postulate a similar coordination for ligand **3** in complex [Fe(**3**)$(OTf)_2]_2$ (see Fig. 5). Coordination *via* the carbonyl oxygen donor is clearly preferred over coordination by the weakly basic amide nitrogen donors. In acetonitrile, formation of acetonitrile-coordinated complexes occurs and the triflate anions are not coordinated to the metal centre in the temperature range from 233–343 K, as shown by a single peak between −70 and −80 ppm in the VT-^{19}F NMR spectra (see Fig. S9 and S11†). Only a few related dinuclear iron complexes have been reported with non-methylated pyridyl amide and pyridyl ester

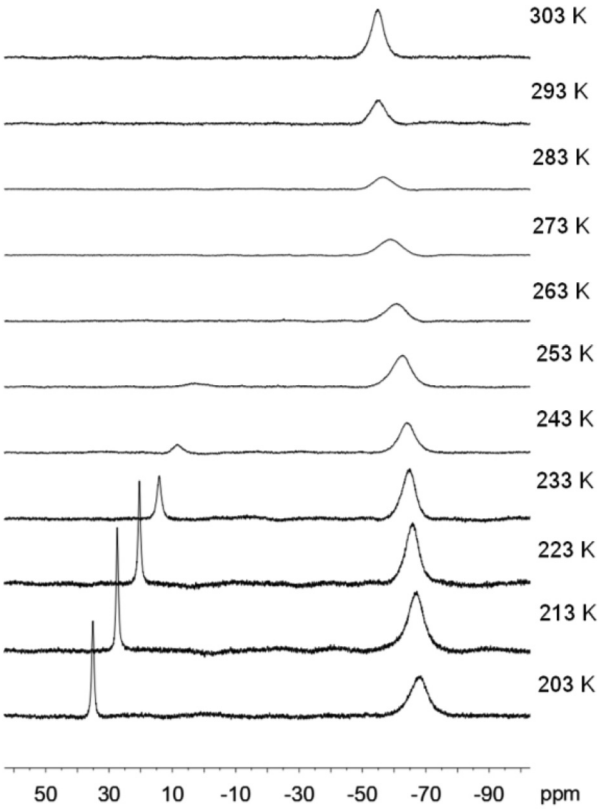

Fig. 6 VT-^{19}F NMR spectra of [Fe(**5**)(OTf)](OTf) in CD_2Cl_2 from 203 to 303 K.

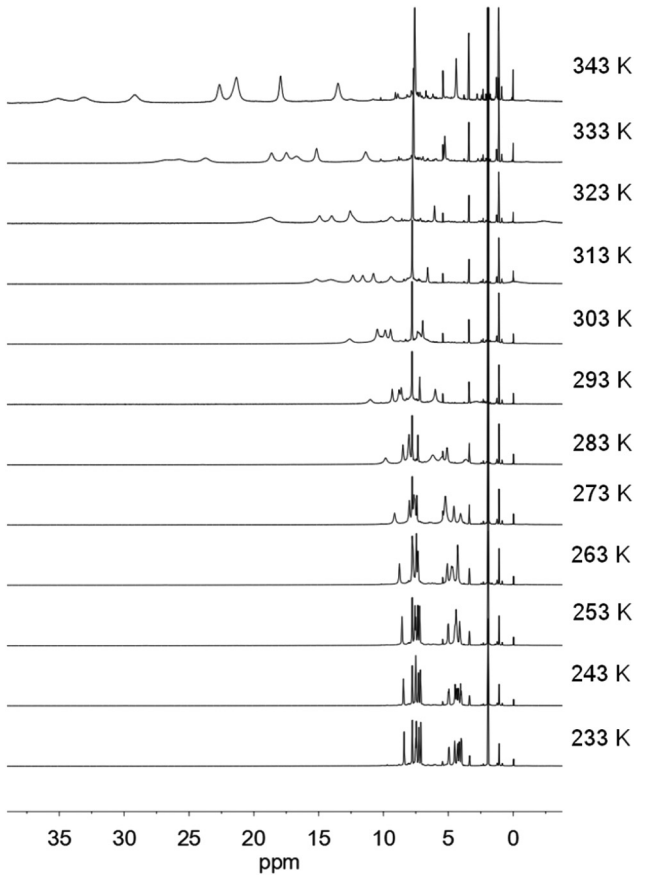

Fig. 7 VT-^{1}H NMR spectra of [Fe(**5**)(OTf)](OTf) in CD_3CN.

ligands.[79–81] Coordination *via* the carbonyl oxygen donors was also seen in a palladium(II) complex containing ligand **3**,[82] which is the only previously reported structure of a metal complex containing **3**.

The six-coordinate octahedral complex [Fe(**5**)(OTf)](OTf) is the major species at low temperature, as indicated by two signals in the ^{19}F NMR spectrum, one for coordinated triflate at 35 ppm and one for non-coordinated triflate anions at −68 ppm at 203 K (Fig. 6). As the temperature is raised, the rate of exchange between coordinated and non-coordinated triflate anions will become faster, but there is also a shift in the equilibrium from a six-coordinate complex $[Fe(\mathbf{5})(OTf)]^+$ to a five-coordinate complex $[Fe(\mathbf{5})]^{2+}$, as illustrated in eqn (2). Both complexes are high spin, as can be seen from the VT ^{1}H NMR spectra in CD_2Cl_2 (Fig. S12†). The two iron(II) complexes are similar to the previously reported six- and five-coordinate zinc(II) complexes with the same pentadentate ligand, $[Zn(\mathbf{5})Cl]^+$ and $[Zn(\mathbf{5})]^{2+}$.[60]

In acetonitrile, the octahedral iron(II) complex $[Fe(\mathbf{5})(CH_3CN)]^{2+}$ is formed with non-coordinating triflate anions (see VT ^{19}F NMR in Fig. S13†). At low temperature this is a low spin complex, which shows SC behaviour as the temperature is increased (see Fig. 7). The HS $[Fe(\mathbf{5})(CH_3CN)]^{2+}$ complex is more labile and the equilibrium will shift between the six-coordinate complex $[Fe(\mathbf{5})(CH_3CN)]^{2+}$ and a five-coordinate complex $[Fe(\mathbf{5})]^{2+}$, resulting in an anomalous magnetic behaviour similar to complex $[Fe(\mathbf{1})(CH_3CN)_2]^{2+}$, as shown by the magnetic moment measurements in Fig. 2(×).

We have previously reported the remarkable coordination behaviour of complex $[Fe(\mathbf{6})(OTf)_2]$, which is distinctly different from [Fe(**5**)(OTf)](OTf). In non-coordinating solvents such as DCM, an equilibrium is observed between a seven-coordinate complex $[Fe(\mathbf{6})(OTf)_2]$ with pentagonal bipyramidal coordination and a five-coordinate trigonal bipyramidal complex $[Fe(\mathbf{6})](OTf)_2$ with two non-coordinating triflate anions (see eqn (3)).[62] In acetonitrile, a seven-coordinate $[Fe(\mathbf{6})(CH_3CN)_2]^{2+}$ complex is formed, which is in equilibrium with the five-coordinate complex $[Fe(\mathbf{6})]^{2+}$. These seven- and five-coordinate complexes are all high spin, as shown by their magnetic moment measurements in Fig. 2(◆), which appears to be the preferred spin state for this complex rather than forming an octahedral LS complex $[Fe(\mathbf{6})(CH_3CN)]^{2+}$.

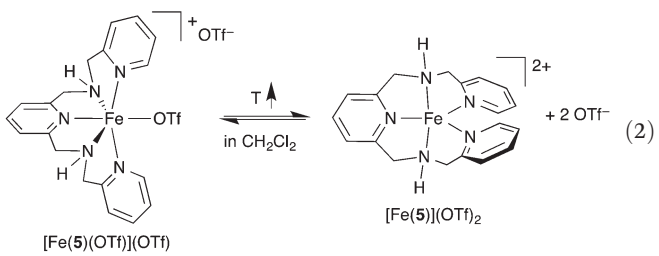

(2)

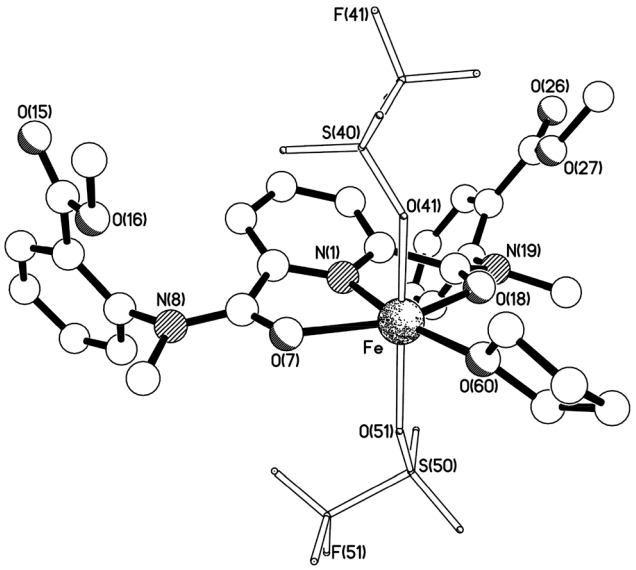

Fig. 8 The crystal structure of [Fe(**8**)(OTf)$_2$(thf)]. Selected bond lengths (Å) and angles (°); Fe–N(1) 2.1259(14), Fe–O(7) 2.1139(12), Fe–O(18) 2.1178(13), Fe–O(41) 2.147(2), Fe–O(51) 2.1081(15), Fe–O(60) 2.091(3), N(1)–Fe–O(7) 74.00(5), N(1)–Fe–O(18) 74.69(5), N(1)–Fe–O(41) 93.66(9), N(1)–Fe–O(51) 98.35(6), N(1)–Fe–O(60) 168.17(16), O(7)–Fe–O(18) 148.67(5), O(7)–Fe–O(41) 89.61(10), O(7)–Fe–O(51) 87.25(6), O(7)–Fe–O(60) 117.74(16), O(18)–Fe–O(41) 93.51(10), O(18)–Fe–O(51) 96.14(6), O(18)–Fe–O(60) 93.59(16), O(41)–Fe–O(51) 166.22(9), O(41)–Fe–O(60) 85.32(14), O(51)–Fe–O(60) 84.29(12).

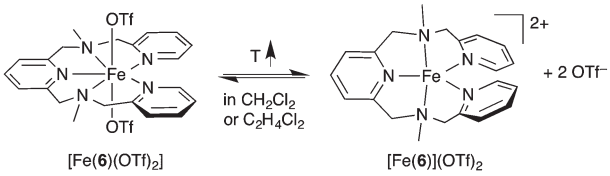

(3)

Iron(II) complexes of the potentially pentadentate ligands **7** and **8** are paramagnetic (see Fig. S14 and S16†) and contain coordinated carbonyl donors according to IR analysis. The ν(C=O) signal of ligand **7** decreases from 1647 to 1603 cm^{-1} upon coordination. Similar changes were observed in a related nickel(II) complex of a pyridine dicarboxamide ligand with coordinated carbonyl oxygens.[83] Attempts to react the non-methylated precursor of ligand **7** with iron(II) bis(triflate) were unsuccessful, probably due to the poor solubility of this precursor. The ^{19}F NMR spectrum of [Fe(**7**)(OTf)$_2$] in CD_3CN indicates non-coordinating triflate anions (Fig. S15†) and the UV-vis spectrum in CH_3CN shows a relatively weak MLCT absorption at 425 nm (ε = 260 M^{-1} cm^{-1}). X-ray analysis of the iron(II) bis(triflate) complex of ligand **8** revealed a tridentate coordination of the ligand *via* the carbonyl oxygen donors with an additional THF ligand to complete the octahedral coordination in [Fe(**8**)(OTf)$_2$(thf)] (see Fig. 8). The iron centre has a severely distorted octahedral geometry with *cis* angles in the range 74.00(5)–117.74(16)°, and the metal atom lies *ca.* 0.74 Å out of the N(1)-pyridyl ring plane. Noteworthy intermolecular interactions are a pair of F···π contacts across independent centres of symmetry. The F(51) triflate fluorine atom in one molecule approaches the N(1) pyridyl ring in a C_i-related counterpart (F···π 3.59 Å), whilst F(41) approaches the N(8)-bound aryl ring across a different centre of symmetry (F···π 3.51 Å), resulting in an extended chain of molecules (interactions **a** and **b** respectively in Fig. S21; see the ESI†). Tridentate coordination of pyridine dicarboxamide ligands *via* the carbonyl oxygens appears to be the dominant coordination mode for nickel, copper and cobalt complexes,[84,85] and based on the available data on the complex with ligand **7**, we postulate a similar coordination mode in this case.

Several conclusions can be drawn from these structural studies. Firstly, the BPMEN ligand appears to have a unique ability to provide a very rigid ligand framework with a *cis*-α coordination mode and a strong binding of the iron centre. Any flexibility in the ligand framework or weakening of the N-donor strength and a consequent weakening of the metal–ligand interaction (*e.g.* ligand **1**) can lead to changes in the coordination behaviour (*cis*-β and *trans* isomers). Secondly, the addition of a pyridine donor in the pentadentate ligands **5** and **6** does not improve the strength of the metal–ligand interaction and disfavours the formation of octahedral complexes. Thirdly, if a pyridylmethylene amine unit is changed to a pyridyl carboxamide unit (ligands **3**, **4**, **7** and **8**), the amide N-donor will be too weak to coordinate effectively and the complexes rearrange to a preferred coordination of another donor.

Catalytic oxidation of cyclohexane

The catalytic properties of the iron(II) bis(triflate) complexes containing ligands **1–8** for the oxidation of cyclohexane with H_2O_2 have been evaluated (eqn (4)).

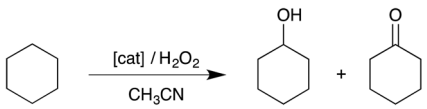

(4)

The oxidation reactions were carried out under our standard conditions in order to compare the results with previously reported data (see ESI†).[48,49] Hydrogen peroxide solution (10 equiv. or 100 equiv.) was added to an acetonitrile solution containing the catalyst (1 equiv.) and cyclohexane (1000 equiv.). A large excess of substrate was used to minimize over-oxidation of cyclohexanol (A) to cyclohexanone (K). The addition of dilute H_2O_2 was carried out slowly using a syringe pump, in order to minimise H_2O_2 decomposition. The yields are based on the amount of oxidant (H_2O_2) converted into oxygenated products. All the individual catalytic runs were performed at least twice.

Catalytic experiments were carried out initially using 10 equiv. of H_2O_2. The amount of cyclohexanol (A) and cyclohexanone (K) are measured by GC and the percentage conversion of H_2O_2 into oxidised products (A + K) for the different catalysts is shown in Table 1. The iron bis(triflate) complex [Fe(BPMEN)(OTf)$_2$] is used as a benchmark against which the other catalysts are compared. We have previously reported that this catalyst, when using 10 equiv. of H_2O_2, converts 65% of the added H_2O_2 into oxygenated products, with a large ratio of

Table 1 Oxidation of cyclohexane with H_2O_2 catalysed by [Fe(L)(OTf)$_2$][a]

Run	Catalyst	Equiv. H_2O_2	A + K[b] (%)	A/K[c]
1[d]	[Fe(BPMEN)(OTf)$_2$]	10	65	9.5
2[d]	[Fe(BPMEN)(OTf)$_2$]	100	48	2.5
2	[Fe(**1**)(OTf)$_2$]	10	23	1.4
2	[Fe(**1**)(OTf)$_2$]	100	4	2.4
3	[Fe(**2**)(OTf)$_2$]	10	37	9.6
4	[Fe(**5**)(OTf)$_2$]	10	22	4.5
5	[Fe(**6**)(OTf)$_2$]	10	25	2.0
6	[Fe(**7**)(OTf)$_2$]	10	5	1.8
7	[Fe(**8**)(OTf)$_2$]	10	19	2.1
8[e]	[Fe(OTf)$_2$(CH$_3$CN)$_2$]	10	4	1.6

[a] Catalytic conditions: see ESI. [b] Total percentage yield of cyclohexanol (A) + cyclohexanone (K), expressed as moles of product per mole of H_2O_2. [c] Ratio of moles of cyclohexanol (A) to moles of cyclohexanone (K). [d] Data taken from ref. 49. [e] Data taken from ref. 89.

cyclohexanol to cyclohexanone (A/K ratio) of 9.[86] These results are consistent with those reported previously by Que and co-workers for the complex [Fe(BPMEN)(CH$_3$CN)$_2$](ClO$_4$)$_2$.[87] The addition of more H_2O_2 (100 equiv.) results in a lower percentage conversion and a lower A/K ratio. The results obtained with [Fe(OTf)$_2$(CH$_3$CN)$_2$] have been added for comparison (run 8), which shows only low conversions and A/K ratios, indicative of Fenton-type behaviour.

The non-methylated complex [Fe(**1**)(OTf)$_2$] shows a lower catalytic conversion and a smaller A/K ratio. This complex was also evaluated using 100 equiv. H_2O_2, showing comparable results to those reported by Shteinman an co-workers, who reported a ratio of A/K = 2 using 140 equiv. H_2O_2.[67] The lower activity of this complex compared to the benchmark catalyst is tentatively ascribed to the ease of ligand degradation in the case of secondary amines. Complex [Fe(**2**)(OTf)$_2$] gave the best conversion and A/K ratio within the series, although still lower compared to [Fe(BPMEN)(OTf)$_2$]. Complex [Fe(**2**)(OTf)$_2$] exists as a mixture of isomers (see Fig. 3) that are likely to have different individual catalytic oxidation activity. Evaluation of the catalytic activity of the individual isomers would require the synthesis of enantiomerically pure ligands and complexes. The complexes [Fe(**3**)(OTf)$_2$] and [Fe(**4**)(OTf)$_2$] with H_2O_2 showed no conversion under these conditions. The pentadentate complexes [Fe(**5**)(OTf)$_2$] and [Fe(**6**)(OTf)$_2$] showed a comparable but moderate conversion and A/K ratios, indicating that the two *cis*-labile sites are not essential for catalytic oxidation activity in these complexes. Relatively low conversions and A/K ratios were observed with complexes [Fe(**7**)(OTf)$_2$] and [Fe(**8**)(OTf)$_2$], where the pyridyl diamides are coordinated as tridentate ligands. Previous experiments using iron(II) complexes with tridentate ligands have shown similar results for the oxidation of cyclohexane.[88]

Catalyst decomposition

Previous studies and the structural analysis carried out here for complexes [Fe(**1**)(OTf)$_2$] and [Fe(**2**)(OTf)$_2$] have shown that changes to the BPMEN ligand framework generally lead to a change in ligand flexibility, such that different coordination modes (*cis*-β and *trans*) become accessible. An increase in ligand flexibility results in complexes that show inferior catalytic activity in alkane oxidation.[48,49,86] As a result of these studies, it has become increasingly clear that catalyst stability, under the harsh oxidising conditions required to oxidise alkanes, is a major factor that determines the catalytic efficiency of a given catalyst. One possible deactivation pathway that has been invoked in a number of related non-heme catalyst systems is the formation of inactive dinuclear μ-oxo iron(III) complexes.[9,10] However, certain dinuclear μ-oxo iron(III) complexes are active alkane hydroxylation catalysts,[90–92] which suggests that dinuclear μ-oxo iron(III) complexes can be in equilibrium with mononuclear iron(III) hydroxo complexes (probably together with other dinuclear μ-oxo/μ-hydroxo intermediates).[93–96] The formation of dinuclear complexes may be minimized by steric congestion around the metal centre.[10,91,97,98] Ligand rigidity, a strong ligand field and low chemical reactivity of the ligand appear to be critically important for the stability and lifetime of non-heme catalysts.

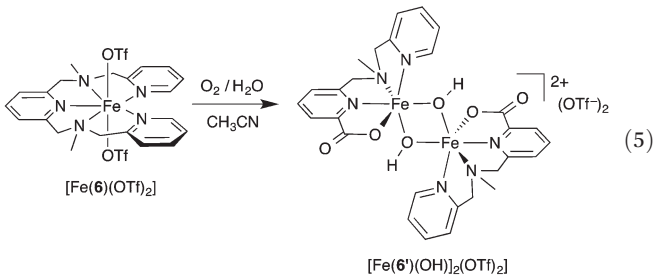

(5)

When complex [Fe(**6**)(OTf)$_2$] was exposed to air and moisture in acetonitrile, oxidative ligand degradation occurred and an isolable complex could be obtained, which was characterised by X-ray diffraction. A dinuclear μ^2-(OH)$_2$-iron(III) complex [Fe(**6′**)(OH)]$_2$(OTf)$_2$ was obtained (see eqn (5) and Fig. 9) with a centre of symmetry in the middle of the Fe_2O_2 ring. The unique iron centre has a distorted octahedral geometry with *cis* angles in the range 73.70(8)–109.25(8)°, and is bound to one tetradentate *N*,*N*′,*N*″,*O* donor ligand as well as to two bridging hydroxo ligands. The Fe–O–Fe bridges are symmetric [Fe(1)–O(20) 1.9664(17), Fe(1A)–O(20) 1.9700(17)] and subtend an angle of 103.40(8)° at the oxygen. The triflate anions sit in the clefts formed by the pyridyl rings on each iron centre with O···centroid separations of *ca.* 3.07 and 3.68 Å (interactions **a** and **b** respectively in Fig. S23†).

The pentadentate ligand **6** has undergone oxidative C–N cleavage to give a picolinate-type ligand **6′**, presumable together with (*N*-methyl)-2-aminomethyl pyridine as the by-product. The iron(II) centre has been oxidised, most likely by oxygen which in turn is reduced and in the presence of moisture results in the formation of hydroxide anions, as observed in complex [Fe(**6′**)(OH)]$_2$(OTf)$_2$. The oxidation of pyridylmethylamine moieties appears to be a common occurrence, sometimes resulting in the formation of stable metal picolinate complexes.[42,44,46,47] Ligand degradation reactions *via* oxidative N-dealkylation was recently observed during catalytic toluene

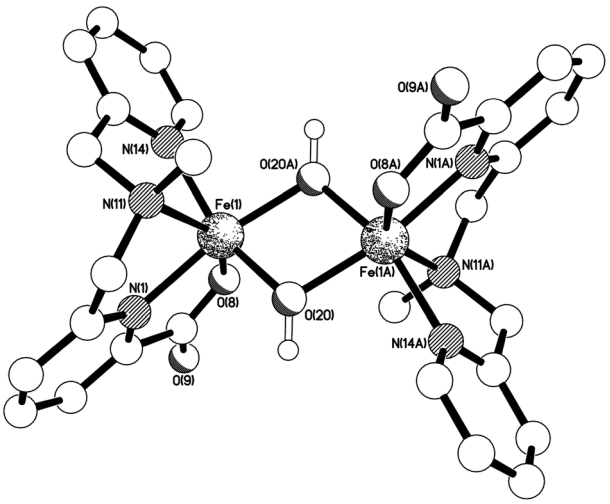

Fig. 9 The structure of the C_i-symmetric di-cation present in the crystal of $[Fe(\mathbf{6}')(OH)]_2(OTf)_2$. Selected bond lengths (Å) and angles (°); Fe(1)–N(1) 2.085(2), Fe(1)–O(8) 1.9728(19), Fe(1)–N(11) 2.247(2), Fe(1)–N(14) 2.111(2), Fe(1)–O(20) 1.9664(17), Fe(1)–O(20A) 1.9700(17), N(1)–Fe(1)–O(8) 77.75(8), N(1)–Fe(1)–N(11) 73.70(8), N(1)–Fe(1)–N(14) 102.22(9), N(1)–Fe(1)–O(20) 93.18(8), N(1)–Fe(1)–O(20A) 169.40(8), O(8)–Fe(1)–N(11) 147.17(8), O(8)–Fe(1)–N(14) 93.70(9), O(8)–Fe(1)–O(20) 103.97(8), O(8)–Fe(1)–O(20A) 101.79(8), N(11)–Fe(1)–N(14) 77.08(8), N(11)–Fe(1)–O(20) 93.55(8), N(11)–Fe(1)–O(20A) 109.25(8), N(14)–Fe(1)–O(20) 158.72(9), N(14)–Fe(1)–O(20A) 88.38(8), O(20)–Fe(1)–O(20A) 76.60(8), Fe(1)–O(20)–Fe(1A) 103.40(8).

oxidation with H_2O_2 with a related iron complex featuring the BPMCN ligand, an analogue of BPMEN with a cyclohexyl backbone.[34]

The mechanism by which oxidative ligand degradation occurs in pyridylamine complexes such as $[Fe(\mathbf{6})(OTf)_2]$ with oxidants is not yet understood, but the results obtained here can be explained according to the general mechanism shown in Scheme 1. Oxidation of a methylene unit in ligand **6** results in a hemi-aminal complex (**B**), which can react further or rearrange to an O-bound hemi-aminal complex **C**. Further oxidation of the tertiary C–H bond in N-bound hemi-aminal complex **B** results in the formation of complex (**E**), which will dehydrate to an amide complex (**F**). As we have seen here for complexes $[Fe(\mathbf{4})(OTf)_2]$ and $[Fe(\mathbf{8})(OTf)_2]$, the weak basicity of amide nitrogen donors will likely result in a rearrangement due de-coordination of the nitrogen donor. Hydrolysis of the amide complex would give a picolinate complex **G**. In the case of complex $[Fe(\mathbf{6})(OTf)_2]$, this results in the picolinate ligand **6′** (see eqn (5)). An alternative pathway involves rearrangement of the N-bound hemi-aminal complex **B** to an O-bound complex of type **C**. Related O-bound hemi-aminal complexes have been isolated and characterised on several occasions.[35–39] Further oxidation and C–N cleavage would also result in the picolinate complex **G**.

In conclusion, ligand degradation in non-heme oxidation catalysts is an important factor that affects catalyst stability and lifetime under the oxidising reaction conditions. In order to investigate potential ligand degradation pathways and to improve catalyst stability, we have prepared a series of iron(II) complexes with tetradentate and pentadentate pyridylamine-type ligands **1–8**. Compared to $[Fe(BPMEN)(OTf)_2]$, all complexes have shown lower activities as catalysts for the oxidation of cyclohexane with H_2O_2 as the oxidant. The BPMEN ligand ensures a strong coordination environment with a *cis*-α geometry at the iron centre, stabilises intermediates in various oxidation states along the catalytic oxidation cycle and undergoes negligible oxidative ligand degradation. The NH donors in $[Fe(\mathbf{1})(OTf)_2]$ provide a weaker ligand field resulting in a conformationally less rigid complex with different geometrical high spin isomers (*cis*-β and *trans* in addition to *cis*-α). Secondary amines are also believed to be more vulnerable to oxidative degradation. A mixture of isomers was obtained in the case of $[Fe(\mathbf{2})(OTf)_2]$, probably with different catalytic activities. Amide donors in ligands **3** and **4** result in dinuclear oxygen-bound complexes with no catalytic activity. Pentadentate ligands in $[Fe(\mathbf{5})(OTf)_2]$ and $[Fe(\mathbf{6})(OTf)_2]$ provide moderate catalytic activity, despite the absence of two *cis*-labile sites, where ligands **7** and **8** were found to coordinate as tridentate ligands and showed only low catalytic activities. The reaction of complex $[Fe(\mathbf{6})(OTf)_2]$ with O_2 has shown that ligand degradation can occur *via* oxidative N-dealkylation, based on the isolation of an iron(III) complex $[Fe(\mathbf{6}')(OH)]_2(OTf)_2$ with a picolinate-type ligand **6′**. We are continuing our efforts to develop robust non-heme iron-based catalysts for the selective oxidation of alkanes.

Experimental section

Starting materials

The following ligands and starting materials have been prepared following literature procedures: *N*,*N*′-dimethyl-bis(2-pyridylmethyl)ethylene diamine (BPMEN),[89] *N*,*N*′-bis(2-pyridylmethyl)ethylene diamine (**1**),[59] *N*,*N*′-dimethyl-bis(2-pyridyl-1-ethyl)ethylene diamine (**2**),[99] *N*,*N*′-dimethyl-*N*,*N*′-bis(2-pyridinecarboxamide)-1,2-ethane (**3**),[64,100] 2,6-bis[(2-pyridylmethyl)-aminomethyl]-pyridine (**5**) and 2,6-bis[(*N*-methyl(2-pyridylmethyl)-amino)methyl]pyridine (**6**),[60,61,101] *N*,*N*′-bis(2-pyridinecarboxamide)-1,2-benzene,[100] 2-*N*,6-*N*-bis(quinolin-8-yl) pyridine-2,6-dicarboxamide.[102] The synthesis of the iron complexes $[Fe(BPMEN)(OTf)_2]$ and $[Fe(\mathbf{6})(OTf)_2]$ has been reported previously.[62,89]

Synthesis of ligands

***N*,*N*′-Dimethyl-*N*,*N*′-bis(2-pyridinecarboxamide)-1,2-benzene (4).** A solution of *N*,*N*′-bis(2-pyridinecarboxamide)-1,2-benzene (1.60 g, 5.03 mmol) in abs. DMF (20 mL) was added dropwise to NaH (362.00 mg, 15.09 mmol) suspended in abs. DMF (20 mL) under inert atmosphere. The mixture was stirred at 40 °C for 50 minutes and then cooled to room temperature. Methyl iodide (0.94 mL, 15.09 mmol) was added and the mixture was stirred at room temperature overnight whereby a brown suspension formed. The solvent was removed under reduced pressure and the residue was extracted with DCM and

water. The organic layer was washed with water and dried over anhydrous $MgSO_4$. The solution was filtered and the solvent was removed under reduced pressure to yield a dark brown/dark red solid as crude product. Column chromatography (ethyl acetate–methanol (90 : 10)) gave pure **4** as beige solid (0.84 g, 48%). ^{1}H-NMR ($CDCl_3$, 400 MHz) (three stereoisomers in a 10 : 6 : 1 ratio) δ (ppm): 3.33 (s, 3/17 of 6H, CH_3), 3.44 (s, 1/17 of 6H, CH_3), 3.56 (s, 3/17 of 6H, CH_3), 3.67 (s, 10/17 of 6H, CH_3), 6.64 (m, 2.8/28 of 12H, Ph-*H*), 6.81 (m, 2.8/28 of 12H, Ph-*H*), 7.02 (br, 0.95/28 of 12H, arom-*H*), 7.17 (m, 4.5/28 of 12H, Py-*H*), 7.32 (br, 0.5/28 of 12H, arom-*H*), 7.35–7.43 (m, 1.9/28 of 12H, arom-*H*), 7.5 (br, 0.5/28 of 12H, arom-*H*), 7.68 (br, 1/28 of 12H, arom-*H*), 7.75 (t, 3.6/28 of 12H, $^3J_{HH}$ = 7.8 Hz, Py-*H*), 7.85 (m, 1.7/28 of 12H, arom-*H*), 7.90 (m, 3.2/28 of 12H, Py-*H*), 8.15 (d, 2.8/28 of 12H, $^3J_{HH}$ = 4.36 Hz, Py-*H*), 8.22 (br, 0.75/28 of 12H, arom-*H*), 8.68 (br, 1/28 of 12H, arom-*H*); ^{13}C-NMR ($CDCl_3$, 400 MHz): (Three stereoisomers in a 10 : 6 : 1 ratio) δ (ppm) = 35 (CH_3), 125 (Py-*C*H), 125 (Py-*C*H), 127 (Ph-*C*H), 129 (Ph-*C*H), 136 (Py-*C*H), 140 (Ph-*C*R), 148 (Py-*C*H), 154 (Py-*C*), 168 (*C*=O); IR: ν (cm^{-1}): 1648 (C=O stretching), 1599 (phenyl), 1586 and 1568 (pyridine), 751 (*ortho*-disubstituted); ESI-MS: *m*/*z* (%): 715 (49) $[M_2 + Na]^+$, 369 (30) $[M + Na]^+$, 347 (100) $[M]^+$.

***N*,*N*′-Bis(dimethyl)-bis(quinolin-8-yl)pyridine-2,6-dicarboxamide (7).** 2-*N*,6-*N*-Bis(quinolin-8-yl)pyridine-2,6-dicarboxamide (2.00 g, 4.77 mmol, 1 eq.) was suspended in ice-cooled (0 °C) DMF (20 mL), to which 60% NaH in mineral oil (572 mg, 14.3 mmol, 3 eq.) was added portion-wise. After 30 minutes of stirring, MeI (2.97 mL, 47.7 mmol, 10 eq.) was added to the yellow mixture and the ice-bath was removed. Stirring was continued at room temperature for 3 h. Water (200 mL) was added (initially dropwise to quench the NaH) and the aqueous layer was extracted with diethyl ether (200 mL) and then chloroform (200 mL). The organic extracts were combined and concentrated *in vacuo*, leaving a yellow DMF residue. Diethyl ether (200 mL) was added followed by pentane (200 mL) and the mixture was left standing at room temperature. After 3 days, yellow crystals had formed, which were collected by filtration and identified as the product by ^{1}H-NMR spectroscopy. Yield: 1.57 g (74%); ^{1}H-NMR (400 MHz, d^6-DMSO): (broad signals) δ (ppm): 8.86 (br s, 2H, 2-Qu*H*), 8.36 (d, 2H, $^3J_{HH}$ = 7.8 Hz, *meta*-Py*H*), 7.89 (d, 2H, $^3J_{HH}$ = 8.4, 7-Qu*H*), 6.55–7.76 (9H, *para*-Py*H* and other Qu*H*), 3.28 (br s, 6H, NCH_3); ^{13}C-NMR (100 MHz, d^6-DMSO): δ (ppm) 168 (*C*=O), 153 (quat. *C*), 151 (2-Qu-*C*H), 143 (quat. *C*), 141 (quat. *C*), 137 (*meta*-Py-*C*H), 129 (*para*-Py-*C*H or other Qu-*C*H), 129 (*para*-Py-*C*H or other Qu-*C*H) 128 (7-Qu*H*), 127 (*para*-Py-*C*H or other Qu-*C*H), 123 (quat. *C*), 122 (*para*-Py-*C*H or other Qu-*C*H) 38 (N*C*H$_3$); ESI-MS: *m*/*z* (%) = 448 (98) $[M + H]^+$, 470 (100) $[M + Na]^+$; IR: ν (cm^{-1}) 1647; Anal. Calcd for $C_{27}H_{21}N_5O_2$: C 72.47, H 4.73, N 15.65, Found: C 71.62, H 4.81, N 15.35.

2,6-Bis[(*N*-methyl-methylanthranilate)carboxamide]pyridine (8). (a) 2,6-Bis[(methylanthranilate)carboxamide]pyridine: 2,6-pyridinedicarbonyl dichloride (1.5 g, 7.4 mmol) were dissolved in abs. toluene. In a second Schlenk flask methyl 2-aminobenzoate (1.4 mL, 14.7 mmol) and triethylamine (2.1 mL, 14.7 mmol) were dissolved in abs. toluene. The second solution was added to the first and the reaction mixture stirred at 80 °C overnight. After cooling the mixture to room temperature, and removal of all volatiles, the residue was taken up in chloroform and saturated aqueous sodium hydrogencarbonate. The phases were separated and the aqueous phase was extracted three times with chloroform. The organic phase was dried over $MgSO_4$, filtered and the solvent removed under reduced pressure. The crude product was recrystallised from chloroform yielding the product as a white solid (2.7 g, 85%). ^{1}H NMR ($CDCl_3$, 400 MHz): δ (ppm) = 12.73 (s, 2H, 2 × N*H*), 8.81 (d, *J* = 8.2 Hz, 2H, 2 × PyH_m), 8.46 (d, *J* = 7.7 Hz, 2H, 2 × ArH_3), 8.14 (t, *J* = 7.8 Hz, 1H, PyH_p), 8.09 (d, *J* = 7.9 Hz, 2H, 2 × ArH_6), 7.64 (t, *J* = 7.8 Hz, 2H, 2 × ArH_5), 7.18 (t, *J* = 7.6 Hz, 2H, 2 × ArH_4), 3.66 (s, 6H, 2 × CH_3). ^{13}C NMR ($CDCl_3$, 101 MHz): δ (ppm) = 167.7, 162.6, 149.4, 140.3, 139.6, 134.4, 131.3, 125.4, 123.6, 121.6, 117.5, 52.2. HRESI-MS: *m*/*z* = 456.1166 $[M + Na]^+$, 434.1342 $[M + H]^+$.

(b) 2,6-Bis[(methylanthranilate)carboxamide]pyridine (700.0 mg, 1.5 mmol) was dissolved in abs. THF and NaH (110.0 mg, 4.6 mmol) were added. After stirring the suspension for 4 h, MeI (0.3 mL, 4.8 mmol) was added and the suspension was stirred at room temperature overnight. After removal of all volatiles at reduced pressure, the residue was taken up in chloroform and saturated aqueous sodium hydrogencarbonate. After the phases were separated the aqueous phase was extracted three times with chloroform. The organic phase was dried over $MgSO_4$, filtered and the solvent removed under reduced pressure. The product **8** was obtained as viscous yellow oil (430 mg, 62%). ^{1}H NMR ($CDCl_3$, 400 MHz) *(due to the presence of three rotamers in a 3 : 2 : 1 ratio, a large number of signals appear at room temperature)*: δ (ppm) = 7.97 (d, *J* = 8.2 Hz, 0.4H), 7.85–7.64 (m, 2.7H), 7.60 (t, *J* = 8.0 Hz, 0.6H), 7.51 (d, *J* = 7.8 Hz, 0.4H), 7.44–7.17 (m, 5.8H), 7.12 (d, *J* = 7.8 Hz, 0.4H), 6.84 (d, *J* = 8.0 Hz, 0.4H), 6.61 (d, *J* = 8.0 Hz, 0.2H), 6.52 (t, *J* = 8.0 Hz, 0.2H), 3.79 (m, 6H), 3.44 (m, 1.5H), 3.29 (m, 3H), 2.89 (m, 1.5H). ^{13}C NMR ($CDCl_3$, 101 MHz): δ (ppm) = 167.8, 167.4, 167.4, 165.9, 165.8, 165.7, 165.6, 152.6, 152.5, 152.2, 151.9, 144.6, 144.0, 143.4, 137.5, 136.3, 134.6, 133.7, 133.1, 133.0, 132.6, 131.5, 131.4, 131.2, 131.1, 130.7, 130.3, 130.1, 128.7, 128.2, 127.8, 127.6, 127.5, 127.4, 124.7, 123.9, 123.7, 123.5, 114.3, 110.7, 52.5, 52.4, 52.2, 51.4, 40.2, 38.7, 38.0, 37.9, 29.7, 29.5. ESI-MS: *m*/*z* = 484 $[M + Na]^+$, 462 $[M + H]^+$.

General synthesis of metal triflate complexes. To prepare $[Fe(\mathbf{L})(OTf)_2]$, the relevant ligand **L** and 1.0 molar equivalent of $[Fe(NCMe)_2(OTf)_2]$ were placed in different Schlenk flasks and dissolved in dry tetrahydrofuran under nitrogen. After adding the solution of the ligand to the suspension of the metal precursor, the reaction mixture was stirred overnight at room temperature. The resulting solution was concentrated to one third of the initial volume. Diethyl ether was added to precipitate the product as solid, which was dried under vacuum.

$[Fe(\mathbf{1})(OTf)_2]$: grey-green solid. 90% yield. ^{1}H NMR (CD_3CN, 400 MHz, 298 K, *all peaks appear as broad singlets*): δ (ppm) =

17.75, 14.87, 13.92, 10.11, 9.83, 6.42, 3.70, 0.66. ^{19}F NMR (CD_2Cl_2) δ −42. MS (FAB, *m*/*z* (%)): 447 (100) [(M − OTf)$^+$], 296 (2) [(M − 2OTf)$^+$]. μ_{eff} (CD_3CN, 298 K) = 2.8 BM. UV-Vis (CH_3CN, 298 K): $\lambda(\varepsilon)$ (nm, M^{-1} cm^{-1}): 375 (4100), 533 (200).

[Fe(**2**)(OTf)$_2$]: yellow solid. 85% yield. Mixture of diastereomers: ^{1}H NMR (CD_3CN) δ 132.6, 73.6, 70.4, 63.3, 59.3, 48.6, 42.2, 41.2, 26.5, 24.4, 18.6, 10.3. ^{19}F NMR (CD_3CN) δ −78.6 ($\nu_{1/2}$ = 900 Hz). ^{19}F NMR (CD_2Cl_2) δ −25.6. MS (+FAB, *m*/*z* (%)): 503 (100) [(M − OTf)$^+$]. μ_{eff} (CD_3CN) = 4.39μ_B. UV-Vis (CH_3CN, 298 K): $\lambda(\varepsilon)$ (nm, M^{-1} cm^{-1}): 376 (3600), 515 (30); Anal. Calcd for $C_{20}H_{26}F_6FeN_4O_6S_2$: C, 36.82; H, 4.02; N, 8.59. Found: C, 36.87; H, 3.96; N, 8.59.

[Fe(**3**)(OTf)$_2$]: yellow solid (1.03 g, 94%). ^{1}H-NMR (CD_3CN, 400 MHz, 298 K) δ (ppm): −1.01, 7.21, 10.25, 18.54, 23.62, 48.96, 66.30, 74.04; ^{19}F-NMR (CD_3CN, 376 MHz, 298 K) δ (ppm): −65.4; UV-Vis (CH_3CN, 298 K): $\lambda(\varepsilon)$ (nm, M^{-1} cm^{-1}): 217 (12 000), 264 (9500), 414 (750); IR: ν (cm^{-1}) 1608 (C═O), 1590 and 1572 (pyridine); LSIMS: *m*/*z* (%): 1155 (2.5) [M_2 − OTf]$^+$, 503 (71.3) [M − OTf]$^+$. Anal. Calcd for $C_{18}H_{18}F_6FeN_4O_8S_2$: C, 33.14; H, 2.78; N, 8.59. Found: C, 33.29; H, 2.88; N, 8.46.

[Fe(**4**)(OTf)]: orange solid (0.83 g, 82%). ^{1}H-NMR (CD_3CN, 400 MHz, 298 K): ∼45 signals indicative of multiple species; ^{19}F-NMR (CD_3CN, 376 MHz): δ (ppm): −59.44. UV-Vis (CH_3CN): $\lambda(\varepsilon)$ (nm, M^{-1} cm^{-1}) = 217(12 000), 262(6800), 416 (500); IR: ν (cm^{-1}): 1610 (C═O), 1585 and 1565 (pyridine). LSIMS: *m*/*z* (%): 1251 (20.9) [M_2 − OTf]$^+$, 551 (100) [M − OTf]$^+$. Anal. calcd for $C_{22}H_{18}F_6FeN_4O_8S_2$: C, 37.73; H, 2.59; N, 8.00. Found: C, 37.81; H, 2.49; N, 7.94. Crystals suitable for X-ray analysis were grown from an acetonitrile solution layered with diethyl ether at room temperature. *Crystal data for* [Fe(**4**)-(OTf)$_2$]$_2$: $C_{44}H_{36}F_{12}Fe_2N_8O_{16}S_4$·2MeCN, M = 1482.86, rhombohedral, $R\bar{3}c$ (no. 167), a = b = 25.4174(4), c = 51.8599(7) Å, V = 29 015.1(8) Å^3, Z = 18 (C_2 symmetry), D_c = 1.528 g cm^{-3}, μ(Mo-Kα) = 0.684 mm^{-1}, T = 173 K, orange/red needles, Oxford Diffraction Xcalibur 3 diffractometer; 9380 independent measured reflections (R_{int} = 0.0293), F^2 refinement,[103] R_1(obs) = 0.0396, wR_2(all) = 0.1164, 6515 independent observed absorption-corrected reflections [$|F_o| > 4\sigma(|F_o|)$, $2\theta_{max}$ = 63°], 390 parameters. CCDC 995554.

[Fe(**5**)(OTf)](OTf): purple solid, 58% yield. ^{1}H NMR (CD_3CN, 400 MHz, 298 K, *all peaks appear as broad singlets*): δ (ppm) = 10.91, 9.25, 8.72, 8.57, 8.20, 7.80, 7.45, 7.33, 7.22, 5.05, 4.69, 4.59, 2.94, 2.50. ^{19}F NMR (CD_3CN, 376 MHz, *broad singlet*): δ (ppm) = −77.76. UV/Vis (CH_3CN): $\lambda(\varepsilon)$ (nm, M^{-1} cm^{-1}): 546 (1000), 381 (7400), 283 (5200). μ_{eff} (CD_3CN, 298 K) = 1.74 BM. LSIMS *m*/*z* = 524 [M − OTf]$^+$. Anal. Calcd (found) for $C_{21}H_{21}F_6FeN_5O_6S_2$: %C 37.46 (37.51), %H 3.14 (3.05), %N 10.40 (10.35).

[Fe(**7**)(OTf)$_2$]: red solid. Yield: 146 mg (74%); ^{1}H-NMR (400 MHz, CD_3CN, 298 K): peaks are overlapping and too broad to assign; ^{19}F-NMR (376 MHz, CD_3CN): δ (ppm) −70 (s, 3F, $^-OSO_2CF_3$). IR: ν (cm^{-1}) 2983, 1603, 1566, 1498, 1400, 1318, 1267, 1213, 1148, 1026, 924, 878, 837, 800, 766, 737, 688. UV-Vis (CH_3CN): $\lambda(\varepsilon)$ (nm, M^{-1} cm^{-1}): 296 (3000), 425 (260). LSIMS: *m*/*z* (%) = 652 (10) [M − OTf]$^+$.

[Fe(**8**)(thf)(OTf)$_2$]: red solid, 81% yield. ^{1}H NMR (CD_2Cl_2, 400 MHz, 298 K, *all peaks appear as broad singlets*): δ (ppm) = 67.11, 65.51, 30.53, 28.47, 26.78, 8.56, 8.42, 8.00, 7.87, 7.68, 6.81, 6.44, 6.06, 5.55, 5.33, 5.10, 4.07, 3.79. ^{19}F NMR (CD_2Cl_2, 376 MHz, *broad singlet*): δ (ppm) = −29. LSIMS *m*/*z* = 666 [M − OTf]$^+$. Anal. Calcd (found) for $C_{21}H_{19}F_6FeN_3O_6S_4$: %C 42.00 (41.92), %H 3.41 (3.35), %N 4.74 (4.44). UV/Vis (CH_3CN): $\lambda(\varepsilon)$ (nm, M^{-1} cm^{-1}): 279 (4200). Crystals suitable for X-ray analysis were grown from a tetrahydrofuran solution at room temperature. *Crystal data for* [Fe(**8**)(OTf)$_2$(thf)]: $C_{31}H_{31}F_6FeN_3O_{13}S_2$, M = 887.56, triclinic, $P\bar{1}$ (no. 2), a = 12.1402(4), b = 12.1595(4), c = 13.5926(3) Å, α = 81.615(2), β = 70.378(3), γ = 88.442(3)°, V = 1869.29(10) Å^3, Z = 2, D_c = 1.577 g cm^{-3}, μ(Mo-Kα) = 0.612 mm^{-1}, T = 173 K, orange/red blocks, Oxford Diffraction Xcalibur 3 diffractometer; 12 149 independent measured reflections (R_{int} = 0.0184), F^2 refinement,[103] R_1(obs) = 0.0473, wR_2(all) = 0.1310, 9276 independent observed absorption-corrected reflections [$|F_o| > 4\sigma(|F_o|)$, $2\theta_{max}$ = 65°], 581 parameters. CCDC 995555.

[Fe(**6′**)(OH)]$_2$(OTf)$_2$: brown crystals were obtained from a solution of [Fe(**6**)(OTf)$_2$] in acetonitrile, upon exposure to air for several days. *Crystal data for* [Fe(**6′**)(OH)]$_2$(OTf)$_2$: $C_{28}H_{30}Fe_2N_6O_6$·2(CF_3SO_3)·2MeCN, M = 1038.53, triclinic, $P\bar{1}$ (no. 2), a = 9.0685(5), b = 9.9914(4), c = 13.1697(5) Å, α = 104.096(3), β = 109.381(4), γ = 98.362(4)°, V = 1057.85(9) Å^3, Z = 1 (C_i symmetry), D_c = 1.630 g cm^{-3}, μ(Cu-Kα) = 7.283 mm^{-1}, T = 173 K, brown plates, Oxford Diffraction Xcalibur PX Ultra diffractometer; 4080 independent measured reflections (R_{int} = 0.0273), F^2 refinement,[103] R_1(obs) = 0.0417, wR_2(all) = 0.1193, 3607 independent observed absorption-corrected reflections [$|F_o| > 4\sigma(|F_o|)$, $2\theta_{max}$ = 145°], 327 parameters. CCDC 995556.

Acknowledgements

We are grateful to the Department of Chemistry for funding and to the IDEA League program for a bursary to IdW.

References

1 T. J. Collins, *Acc. Chem. Res.*, 1994, **27**, 279–385.
2 E. Nagababu and J. M. Rifkind, *Antioxid. Redox Signaling*, 2004, **6**, 967–978.
3 T. Matsui, M. Unno and M. Ikeda-Saito, *Acc. Chem. Res.*, 2010, **43**, 240–247.
4 I. D. Cunningham, T. N. Danks, J. N. Hay, I. Hamerton and S. Gunathilagan, *Tetrahedron*, 2001, **57**, 6847–6853.
5 I. D. Cunningham, T. N. Danks, J. N. Hay, I. Hamerton, S. Gunathilagan and C. Janczak, *J. Mol. Catal.*, 2002, **185**, 25–31.
6 I. D. Cunningham, T. N. Danks, K. T. A. O'Connell and P. W. Scott, *J. Chem. Soc., Perkin Trans. 2*, 1999, 2133–2139.
7 A. C. Serra, E. C. Marçalo and A. M. d. A. Rocha Gonsalves, *J. Mol. Catal.*, 2004, **215**, 17–21.

8 N. A. Stephenson and A. T. Bell, *J. Am. Chem. Soc.*, 2005, **127**, 8635–8643.
9 N. A. Vermeulen, M. S. Chen and M. C. White, *Tetrahedron*, 2009, **65**, 3078–3084.
10 L. Gómez, I. Garcia-Bosch, A. Company, J. Benet-Buchholz, A. Polo, X. Sala, X. Ribas and M. Costas, *Angew. Chem., Int. Ed.*, 2009, **48**, 5720–5723.
11 S. J. Lange, H. Miyake and L. Que Jr., *J. Am. Chem. Soc.*, 1999, **121**, 6330–6331.
12 Y. Mekmouche, S. Ménage, C. Toia-Duboc, M. Fontecave, J.-B. Galey, C. Lebrun and J. Pécaut, *Angew. Chem., Int. Ed.*, 2001, **40**, 949–952.
13 A. Nielsen, F. B. Larsen, A. D. Bond and C. J. McKenzie, *Angew. Chem., Int. Ed.*, 2006, **45**, 1602–1606.
14 A. M. Calafat and L. G. Marzilli, *Inorg. Chem.*, 1993, **32**, 2906–2911.
15 M. Yashiro, T. Mori, M. Sekiguchi, S. Yoshikawa and S. Shiraishi, *J. Chem. Soc., Chem. Commun.*, 1992, 1167–1168.
16 B. Sonnberger, P. Hühn, A. Waßerburger and F. Wasgestian, *Inorg. Chim. Acta*, 1992, **196**, 65–71.
17 M. R. Bukowski, S. Zhu, K. D. Koehntop, W. W. Brennessel and L. Que Jr., *J. Biol. Inorg. Chem.*, 2004, **9**, 39–48.
18 M. Yamaguchi, M. Saburi and S. Yoshikawa, *J. Am. Chem. Soc.*, 1984, **106**, 8293–8295.
19 K. Jitsukawa, T. Yamamoto, T. Atsumi, H. Masuda and H. Einaga, *J. Chem. Soc., Chem. Commun.*, 1994, 2335–2336.
20 M.-C. Rodríguez, F. Lambert, I. Morgenstern-Badarau, M. Cesario, J. Guilhem, B. Keita and L. Nadjo, *Inorg. Chem.*, 1997, **36**, 3525–3531.
21 R. M. Hartshorn, *J. Chem. Soc., Dalton Trans.*, 2002, 3214–3218.
22 I. Sanyal, M. Mahroof-Tahir, M. S. Nasir, P. Ghosh, B. I. Cohen, Y. Gultneh, R. W. Cruse, A. Farooq, K. D. Karlin, S. Liu and J. Zubieta, *Inorg. Chem.*, 1992, **31**, 4322–4332.
23 D. Lee and S. J. Lippard, *J. Am. Chem. Soc.*, 2001, **123**, 4611–4612.
24 D. Lee and S. J. Lippard, *Inorg. Chem.*, 2002, **41**, 827–837.
25 E. C. Carson and S. J. Lippard, *J. Inorg. Biochem.*, 2006, **100**, 1109–1117.
26 A. Böttcher, H. Elias, E.-G. Jäger, H. Langfelderova, M. Mazur, L. Müller, H. Paulus, P. Pelikan, M. Rudolph and M. Valko, *Inorg. Chem.*, 1993, **32**, 4131–4138.
27 S. Zhu, W. W. Brennessel, R. G. Harrison and L. Que Jr., *Inorg. Chim. Acta*, 2002, **337**, 32–38.
28 J. M. Rowland, M. M. Olmstead and P. K. Mascharak, *Inorg. Chem.*, 2001, **41**, 2754–2760.
29 M. Renz, C. Hemmert, B. Donnadieu and B. Meunier, *Chem. Commun.*, 1998, 1635–1636.
30 M. Renz, C. Hemmert, H. Gornitzka and B. Meunier, *New J. Chem.*, 1999, **23**, 773–776.
31 C. Hemmert, M. Renz, H. Gornitzka, S. Soulet and B. Meunier, *Chem. – Eur. J.*, 1999, **5**, 1766–1774.
32 M. Ostermeier, C. Limberg, B. Ziemer and V. Karunakaran, *Angew. Chem., Int. Ed.*, 2007, **46**, 5329–5331.
33 H. Kooijman, S. Tanase, E. Bouwman, J. Reedijk and A. L. Spek, *Acta. Crystallogr., Sect. C: Cryst. Struct. Commun.*, 2006, **62**, m510–m512.
34 M. Canals, R. Gonzalez-Olmos, M. Costas and A. Company, *Environ. Sci. Technol.*, 2013, **47**, 9918–9927.
35 N. Arulsamy and D. J. Hodgson, *Inorg. Chem.*, 1994, **33**, 4531–4536.
36 V. M. Ugalde-Saldívar, M. E. Sosa-Torres, L. Ortiz-Frade, S. Bernès and H. Höpfl, *J. Chem. Soc., Dalton Trans.*, 2001, 3099–3107.
37 Z. Liu, H. Kooijman, A. L. Spek and E. Bouwman, *Prog. Org. Coat.*, 2007, **60**, 343–349.
38 J. P. Saucedo-Vázquez, V. M. Ugalde-Saldívar, A. R. Toscano, P. M. H. Kroneck and M. E. Sosa-Torres, *Inorg. Chem.*, 2009, **48**, 1214–1222.
39 S. K. Padhi, R. Sahu and V. Manivannan, *Inorg. Chim. Acta*, 2011, **367**, 57–63.
40 L. You, S. R. Long, V. M. Lynch and E. V. Anslyn, *Chem. – Eur. J.*, 2011, **17**, 11017–11023.
41 P. Comba, S. Kuwata, G. Linti, H. Pritzkow, M. Tarnai and H. Wadepohl, *Chem. Commun.*, 2006, 2074–2076.
42 S. Groni, P. Dorlet, G. Blain, S. Bourcier, R. Guillot and E. Anxolabéhère-Mallart, *Inorg. Chem.*, 2008, **47**, 3166–3172.
43 A. Thibon, J.-F. Bartoli, S. Bourcier and F. Banse, *Dalton Trans.*, 2009, 9587–9594.
44 D. Pijper, P. Saisaha, J. W. de Boer, R. Hoen, C. Smit, A. Meetsma, R. Hage, R. P. van Summeren, P. L. Alsters, B. L. Feringa and W. R. Browne, *Dalton Trans.*, 2010, **39**, 10375–10381.
45 S. Mahapatra, V. G. Young Jr., S. Kaderli, A. D. Zuberbühler and W. B. Tolman, *Angew. Chem., Int. Ed. Engl.*, 1997, **36**, 130–133.
46 M. S. Vad, A. Nielsen, A. Lennartson, A. D. Bond, J. E. McGrady and C. J. McKenzie, *Dalton Trans.*, 2011, **40**, 10698–10707.
47 D. G. Lonnon, D. C. Craig and S. B. Colbran, *Inorg. Chem. Commun.*, 2003, **6**, 1351–1353.
48 J. England, G. J. P. Britovsek, N. Rabadia and A. J. P. White, *Inorg. Chem.*, 2007, **46**, 3752–3767.
49 J. England, C. R. Davis, M. Banaru, A. J. P. White and G. J. P. Britovsek, *Adv. Synth. Catal.*, 2008, **350**, 883–897.
50 J. England, R. Gondhia, L. Bigorra-Lopez, A. R. Petersen, A. J. P. White and G. J. P. Britovsek, *Dalton Trans.*, 2009, 5319–5334.
51 K. Chen and L. Que Jr., *Chem. Commun.*, 1999, 1375–1376.
52 G. Xue, D. Wang, R. De Hont, A. T. Fiedler, X. Shan, E. Münck and L. Que Jr., *Proc. Natl. Acad. Sci. U. S. A.*, 2007, **104**, 20713–20718.
53 M. Goto, M. Takeshita, N. Kanda, T. Sakai and V. L. Goedken, *Inorg. Chem.*, 1985, **24**, 582–587.
54 V. L. Goedken and D. H. Busch, *J. Am. Chem. Soc.*, 1972, **94**, 7355–7340.

55 G. J. Christian, A. Llobet and F. Maseras, *Inorg. Chem.*, 2010, **49**, 5977–5985.
56 C. Hemmert, A. P. Maestrin, M. Renz, H. Gornitzka and B. Meunier, *C. R. Acad. Sci., Ser. C*, 2000, **3**, 735–741.
57 M. Wu, C.-X. Miao, S. Wang, X. Hu, C. Xia, F. E. Kühn and W. Sun, *Adv. Synth. Catal.*, 2011, **353**, 3014–3022.
58 T. M. Suzuki, T. Kimura and J. Fujita, *Bull. Chem. Soc. Jpn.*, 1980, **53**, 77–81.
59 H. A. Goodwin and F. Lions, *J. Am. Chem. Soc.*, 1960, **82**, 5013–5023.
60 T. Darbre, C. Dubs, E. Rusanov and H. Stoeckli-Evans, *Eur. J. Inorg. Chem.*, 2002, 3284–3291.
61 G. R. Newkome, V. K. Gupta, F. R. Fronczek and S. Pappalardo, *Inorg. Chem.*, 1984, **23**, 2400–2408.
62 M. Grau, J. England, R. Torres Martin de Rosales, H. S. Rzepa, A. J. P. White and G. J. P. Britovsek, *Inorg. Chem.*, 2013, **52**, 11867–11874.
63 I. Okamoto, M. Terashima, H. Masu, M. Nabeta, K. Ono, N. Morita, K. Katagiri, I. Azumaya and O. Tamura, *Tetrahedron*, 2011, **67**, 8536–8543.
64 A. V. Malkov, L. Gouriou, G. C. Lloyd-Jones, I. Stary, V. Langer, P. Spoor, V. Vinader and P. Kocovsky, *Chem. – Eur. J.*, 2006, **12**, 6910–6929.
65 M. C. White, A. G. Doyle and E. N. Jacobsen, *J. Am. Chem. Soc.*, 2001, **123**, 7194–7195.
66 K. P. Bryliakov, E. A. Duban and E. P. Talsi, *Eur. J. Inorg. Chem.*, 2005, 72–76.
67 E. A. Turitsyna, O. N. Gritsenko and A. A. Shteinman, *Kinet. Catal.*, 2007, **48**, 53–59.
68 S. Kundu, E. Matito, S. Walleck, F. F. Pfaff, F. Heims, B. Rábay, J. M. Luis, A. Company, B. Braun, T. Glaser and K. Ray, *Chem. – Eur. J.*, 2012, **18**, 2787–2791.
69 H. Toftlund, E. Pedersen and S. Yde-Andersen, *Acta Chem. Scand.*, 1984, **38A**, 693–697.
70 J.-F. Létard, S. Asthana, H. J. Shepherd, P. Guionneau, A. E. Goeta, N. Suemura, R. Ishikawa and S. Kaizaki, *Chem. – Eur. J.*, 2012, **18**, 5924–5934.
71 J. G. Gibson and E. D. McKenzie, *J. Chem. Soc.*, 1971 (A), 1666–1683.
72 S. Utsuno, A. Hayashi, S. Kondo and M. Utsumi, *Chem. Lett.*, 1979, 351–352.
73 L. Xu, I. A. Setyawati, J. Pierreroy, M. Pink, V. G. Young Jr., B. O. Patrick, S. J. Rettig and C. Orvig, *Inorg. Chem.*, 2000, **39**, 5958–5963.
74 M. A. Heinrichs, D. J. Hodgson, K. Michelsen and E. Pedersen, *Inorg. Chem.*, 1984, **23**, 3174–3180.
75 J. J. McGarvey, I. Lawthers, K. Heremans and H. Toftlund, *Inorg. Chem.*, 1990, **29**, 252–256.
76 J. K. Beattie, *Adv. Inorg. Chem.*, 1988, **32**, 1–53.
77 S. Schenker, P. C. Stein, J. A. Wolny, C. Brady, J. J. McGarvey, H. Toftlund and A. Hauser, *Inorg. Chem.*, 2001, **40**, 134–139.
78 W. Jacob and R. Mukherjee, *Inorg. Chim. Acta*, 2006, **359**, 4565–4573.
79 L. Yang, R.-N. Wei, R. Li, X.-G. Zhou and J.-L. Zou, *J. Mol. Catal. A: Chem.*, 2007, **266**, 284–289.
80 E. A. Turitsyna and A. A. Shteinman, *Russ. Chem. Bull.*, 2011, **60**, 2094–2099.
81 J. J. Kodanko and S. J. Lippard, *Inorg. Chim. Acta*, 2008, **361**, 894–900.
82 M. W. Mulqi, F. S. Stephens and R. S. Vagg, *Inorg. Chim. Acta*, 1982, **63**, 197–207.
83 J. G. H. du Preez and B. J. A. M. van Brecht, *Inorg. Chim. Acta*, 1989, **162**, 49–56.
84 P. Kapoor, A. P. S. Pannu, M. Sharma, M. S. Hundal and R. Kapoor, *J. Coord. Chem.*, 2010, **63**, 3635–3647.
85 P. Kapoor, A. P. S. Pannu, M. Sharma, G. Hundal, R. Kapoor and M. S. Hundal, *J. Coord. Chem.*, 2011, **64**, 256–271.
86 G. J. P. Britovsek, J. England and A. J. P. White, *Dalton Trans.*, 2006, 1399–1408.
87 K. Chen and L. Que Jr., *J. Am. Chem. Soc.*, 2001, **123**, 6327–6337.
88 G. J. P. Britovsek, J. England, S. K. Spitzmesser, A. J. P. White and D. J. Williams, *Dalton Trans.*, 2005, 945–955.
89 G. J. P. Britovsek, J. England and A. J. P. White, *Inorg. Chem.*, 2005, **44**, 8125–8134.
90 K. Chen and L. Que Jr., *J. Am. Chem. Soc.*, 2001, **123**, 6327–6337.
91 Y. Meckmouche, S. Menage, C. Toia-Duboc, M. Fontecave, J. B. Galey, C. Lebrun and J. Pecaut, *Angew. Chem., Int. Ed.*, 2001, **40**, 949.
92 K. Chen, M. Costas, J. Kim, A. K. Tipton and L. Que Jr., *J. Am. Chem. Soc.*, 2002, **124**, 3026–3035.
93 D. M. Kurtz Jr., *Chem. Rev.*, 1990, **90**, 585–606.
94 S. Poussereau, G. Blondin, M. Cesario, J. Guilhem, G. Chottard, F. Gonnet and J.-J. Girerd, *Inorg. Chem.*, 1998, **37**, 3127–3132.
95 S. Taktak, S. V. Kryatov and E. V. Rybak-Akimova, *Inorg. Chem.*, 2004, **43**, 7196–7209.
96 R. Hazell, K. B. Jensen, C. J. McKenzie and H. Toftlund, *J. Chem. Soc., Dalton Trans.*, 1995, 707.
97 L. Gómez, M. Canta, D. Font, I. Prat, X. Ribas and M. Costas, *J. Org. Chem.*, 2013, **78**, 1421–1433.
98 P. E. Gormisky and M. C. White, *J. Am. Chem. Soc.*, 2013, **135**, 14052–14055.
99 R. P. Halliday, W. J. Kinnard and J. P. Buckley, *J. Pharm. Sci.*, 1964, **53**, 19–23.
100 D. J. Barnes, R. L. Chapman, R. S. Vagg and E. C. Watton, *J. Chem. Eng. Data*, 1978, **23**, 349–350.
101 D. W. Gruenwedel, *Inorg. Chem.*, 1968, **7**, 495–501.
102 K. Hiratani and K. Taguchi, *Bull. Chem. Soc. Jpn.*, 1990, **63**, 3331–3333.
103 (*a*) *SHELXTL*, Bruker AXS, Madison, WI; (*b*) SHELX-97, G. M. Sheldrick, *Acta Crystallogr., Sect. A: Fundam. Crystallogr.*, 2008, **64**, 112–122.